MULTILOOP CONTROL OF TANDEM ACCELERATORS

A MULTILOOP FEEDBACK CONTROL SYSTEM

FOR

TANDEM ELECTROSTATIC ACCELERATORS

By

JOHN EVERETT CAIRNS, B.Eng.

A Thesis

Submitted to the School of Graduate Studies

in Partial Fulfilment of the Requirements

For the Degree

Master of Science

McMaster University

May 1973

MASTER OF SCIENCE (1973)
(Physics)

McMASTER UNIVERSITY
Hamilton, Ontario

TITLE: A Multiloop Control System for Tandem Electrostatic Accelerators

AUTHOR: John Everett Cairns, B.Eng.
(McMaster University, Hamilton, Ontario)

SUPERVISOR: Professor J. A. Kuehner

NUMBER OF PAGES: v,39

SCOPE AND CONTENTS:

The limitations of the conventional control system due to the corona discharge are discussed. An improved system employing a parallel feedback loop to modulate the terminal stripper is described. Finally an experiment is described whereby the performance of this system is measured and compared with the original system performance.

ACKNOWLEDGEMENTS

I would like to thank Professor John Kuehner for his help, understanding and patience. I would also like to thank all the members of the accelerator staff for technical advice and assistance during the course of this work.

TABLE OF CONTENTS

LIST OF FIGURES

Introduction:

One of the most versatile tools of nuclear spectroscopy is the tandem Van de Graaff accelerator. This electrostatic accelerator has the capability of producing continuous beams of particles with high energy resolution over a wide energy range.

Considerable interest has been shown in further improving the energy resolution of such an accelerator[1,2,3]. This interest is mainly directed towards the study of very narrow resonances whose decay are isospin forbidden, and which occur at high excitation energies. A typical example is the $T = 3/2$ analogue resonance in ^{13}N corresponding to the $J^{\pi} = 3/2^{-}$ ground state of ^{13}B[4]. This level has a width of only 1.22 keV[5] resulting from its isospin forbidden decay character. Since the width is very sensitive to isospin impurities it is of considerable intrinsic interest. A necessary requirement for measuring such a width is good beam resolution. Beam resolution is the topic of this thesis. To that end excitation curves are shown for elastic scattering of 14 MeV protons on ^{12}C forming the above mentioned level, not as a study of this level, but as a measure of the beam resolution.

This thesis is divided into three chapters. The first of these concerns general considerations. Here the effects of finite beam energy width and the causes of such width are discussed. From these considerations a new control system is proposed to improve the beam resolution. The second chapter consists of a more detailed description of this control system as it has been built for use on the McMaster FN tandem. The third and final chapter describes experiments to test this control system.

CHAPTER I

GENERAL CONSIDERATIONS

An appreciable fraction of the information obtained in nuclear spectroscopy results from studies of resonant reactions. In the vicinity of an isolated narrow resonance superimposed on a slowly changing background, the reaction crossection has the general form

$$\sigma(E) = A + B \sin(2\beta+\phi),$$

where $\sigma(E)$ represents the energy differential crossection, A, B, ϕ are constants, and

$$\beta = \tan^{-1}(\Gamma/2(E-ER)).$$

Here Γ and ER are the resonance width and energy.

In the limiting case of an infinitesimal target slice, the beam energy is not degraded in passing through this slice. The resulting infinitesimal yield is then proportional to the integral over all beam particle energies of σdx, where dx is the depth of the slice.

$$dY(E) \propto dx \int_0^\infty \sigma(E')G(E - E')dE'$$

where G(E) is the beam resolution function normalized such that

$$\int_0^\infty G(E)dE = 1.$$

The total yield is then proportional to the integral of the differential yield over the target thickness:

$$Y(E) = \int_{o}^{x} \int_{o}^{\infty} \sigma(E')G(E^{(x)} - E')dE'dx$$

$$= \int_{E}^{E-\Delta} \int_{o}^{\infty} \sigma(E')G(E'' - E')dE'dE''$$

where Δ is the total energy loss of the beam in passing through the target. In the above discussion it is assumed that the energy varies directly with the depth, x, into the target. Secondary effects such as straggling and channeling are ignored.

The above expression can be written in terms of an overall resolution function by changing the order of the integration

$$Y(E) = \int_{o}^{\infty} \sigma(E')F(E' - E)dE'$$

where

$$F(E) \equiv \int_{E}^{E-\Delta} G(E'')dE'' .$$

Even in this favourable case where one only wishes to populate efficiently and selectively the resonance at energy ER, it is desirable that the full width at half maximum (FWHM) of F(E) be less than Γ, the resonance width.

The contribution to F(E) from Δ, the target thickness, is in a sense not at one's disposal, since for small Δ, the yield is proportional to Δ. However, the contribution from the beam resolution could ideally be made vanishingly small.

Frequently, as in the study of isospin forbidden transitions, one is interested in determining the form of $\sigma(E)$. The width of the resonance is determined by its decay lifetime through the uncertainty relation. The situation is analagous to the Q value in a tuned electronic circuit. In the nuclear analogue, however, energy is lost from the resonant system by means of decay processes such as particle and gamma emission. The resonant width is then an important piece of information in understanding how the resonant level decays, and hence its particular character.

It is useful to be able to calculate how the error in Y(E) propogates to $\sigma(E)$ in order to quantitatively assess the improvement obtained by reducing the width of F(E). A direct approach to this problem results in a lengthy numerical calculation of restricted application. This approach is discussed in Appendix A. The effect of the resolution function is more readily seen by approximating the crossection and resolution functions as Gaussians:

$$\sigma(E) = \frac{1}{0.6\sqrt{\pi}\,\Gamma} \; e^{-E^2/(.6\Gamma)^2}$$

$$F(E) = \frac{1}{0.6\sqrt{\pi}\,\Gamma_F} \; e^{-E^2/(.6\Gamma_F)^2}$$

where Γ and Γ_F are the respective full widths at half maximum. Then the yield as a function of energy is also a Gaussian FWHM Γ_Y such that $\Gamma_Y{}^2 = \Gamma^2 + \Gamma_F{}^2$. Hence by partial differentiation:

$$S[\Gamma] = \left\{ (\frac{\Gamma_Y}{\Gamma})^2 \; S^2[\Gamma_Y] + (\frac{\Gamma_F}{\Gamma})^2 \; S^2[\Gamma_F] \right\}^{1/2}$$

where $S^2[x]$ is the variance of x. For the region frequently of interest $\Gamma_F \approx \Gamma$. It is then seen from the above expression

$$\frac{\partial S[\Gamma]/\partial(\Gamma_F/\Gamma)}{S[\Gamma]} = (\frac{\Gamma_F}{\Gamma}) \; (\frac{S^2[\Gamma_Y] + S^2[\Gamma_F]}{S^2[\Gamma]}) \approx 1$$

$$\partial S[\Gamma]/\partial S[\Gamma_Y] = (\frac{\Gamma_Y}{\Gamma})^2 \; \frac{S[\Gamma_Y]}{S[\Gamma]} \approx 1 \; .$$

Then a factor of N improvement in the beam resolution as measured by Γ_F, is equivalent to a factor of N improvement in the determination of Γ_Y. Since Γ_Y is the width at half maximum of a peak whose height h is subject to Poisson statistics where $S[h] \propto \sqrt{h}$ this is equivalent to a factor of N^2 in data collecting time. As will be shown empirically N can be nearly two, resulting in a significant economy in beam time.

Although not intended as rigorous nor complete, these conditions should be sufficient to indicate the desirability of improving the beam resolution.

The essential operating features of a tandem Van de Graaff accelerator are shown in figure 1. A high voltage

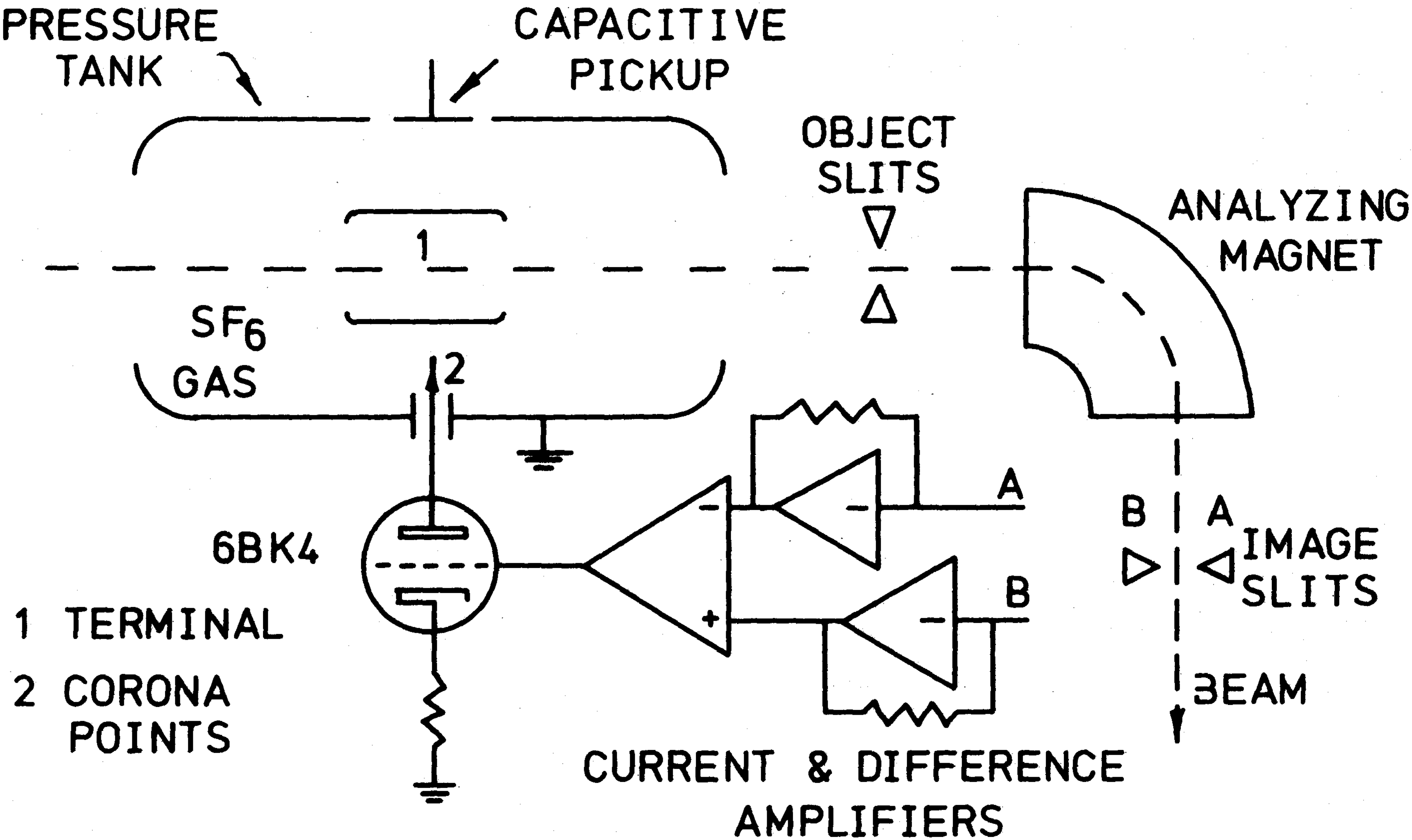

FIG.1 THE TANDEM ACCELERATOR

terminal, (2), is positively charged by means of a constant current supply which sprays charge onto a continuous rubberized belt (not shown). This belt delivers a current to the terminal equal to that flowing out in the column resistors (not shown), the beam (dotted line) and the corona discharge. Negative ions enter from the left, (the dotted line), and are accelerated to the terminal by the positive voltage gradient. Here they enter the drift space within the terminal and pass through either a thin foil or tenuous gas, stripping off electrons to produce positive ions. These positive ions emerge from the terminal and are accelerated to ground by the negative voltage gradient. The beam of ions passes through a set of object slits and is deflected through a momentum analyzing magnet. The dispersion of the magnet is $\Delta x = 4\rho \frac{\Delta P}{P}$, where Δx is the displacement in inches at the image slits for a momentum change ΔP in P, and ρ the radius of curvature is 40 inches. The magnetic field is set for the desired energy E such that any deviation ΔE from E produces a current imbalance on the set of image slits A,B. This difference signal is used to vary the field emission of a set of corona points (2) in the SF_6 insulating gas, and thus to regulate the terminal voltage.

An important characteristic of the SF_6 gas is that it efficiently attaches electrons to form negative ions. Although this property creates an effective insulating medium, it also produces an undesirable time delay in the control loop due to drift time of the negative ions from the corona points to the terminal.Previous measurements[1,2] have determined a transit time of ∿ 12 ms for N_2-CO_2 insulating gas and ∿ 25 ms for SF_6 in "FN" tandems. This delay is essentially constant, since one adjusts the distance from the corona point to the terminal to maintain a constant corona current bias level independent of the terminal voltage. The phase shift associated with this delay combines with the 90° phase shift due to the terminal capacity to cause oscillation of the feedback system. For a SF_6 filled FN tandem the characteristic frequency is ∿15 Hz. Since stable operation then implies unity gain or less at this frequency, one is limited to an order of magnitude attenuation of terminal voltage fluctuations at 2 Hz, the belt frequency. Non-uniformities in the belt produce typical open loop voltage fluctuations of 10 to 20 kv at this frequency. If protons are accelerated, one is then left with 2 to 4 keV modulation of the beam energy resulting from the regulated terminal voltage fluctuations.

Since this contribution to the overall beam resolution is essentially insurmountable as long as the control loop must pass through the corona, there is some advantage to applying an open loop correction voltage to the target as done by Dzubay[6] et al. This approach works very well and gives an overall resolution similar to the system about to be described. Since it is an open loop system, however, it has the severe limitation of requiring an auxiliary analyzing magnet to drive a signal rigorously proportional to the beam energy fluctuations.

An alternate approach, and the one discussed in this thesis, is to improve the control loop by bypassing the corona. This is done by modulating the stripper using a high voltage amplifier in the terminal. A similar technique has been employed on the ion source of a single ended Van de Graaff by Bloch et al[3]. The control signal is transmitted to the terminal amplifier on a modulated light beam from a light emitting diode. This system has several desirable features:

a) It does not require expensive or heavy equipment as does target modulation.
b) The target area is free of any restrictions imposed by the necessity of applying high voltage to the target.
c) This proposed system can be applied directly to magnetic spectrograph experiments. In this case target modulation would unfortunately modulate the outgoing particles as well.
d) Finally, an improved control loop is to be preferred as it eliminates any beam transport problems associated with the energy fluctuations.

However this technique is not without its difficulties. During sparking of the accelerator, severe overvoltages can be developed in the terminal amplifier. The necessity of taking the output to the stripper canal is the greatest problem. Nevertheless a prototype amplifier employing a miniature 10 kV rated output tube had a lifetime of several months under reasonable operating conditions, demonstrating that this problem can be overcome.

With the addition of this "miniature tandem" within the terminal drift space the control system can be represented in block form as shown in figure 2. The detailed circuit is shown in figures 3 and 4.

In figure 2, Δi represents a fluctuation in the net charging current. This leads to an open loop voltage fluctuation ΔV_o. The quantity G is constant over the range of frequencies of interest here, representing a dimensional scale factor relating the energy at the slits to the terminal voltage. The complex quantities $H(\omega)$ and $H'(\omega)$ represent the transfer functions (see Appendix B) of the corona and AC feedback loops shown in figures 3 and 4. R_t and R_e are the regulation factors for the terminal voltage and beam energy, respectively, and are defined as:

$$R_t = \frac{\Delta V_t}{\Delta V_{t_o}} \qquad R_e = \frac{\Delta E}{\Delta E_o}$$

where the subscript "o" refers to an open loop quantity.

It is important to note that the beam energy no longer depends solely on the terminal voltage, as the AC loop adds a corrective voltage in series with the terminal voltage. The usual capacitive pickup monitoring the terminal voltage then does not give sufficient information concerning the machine

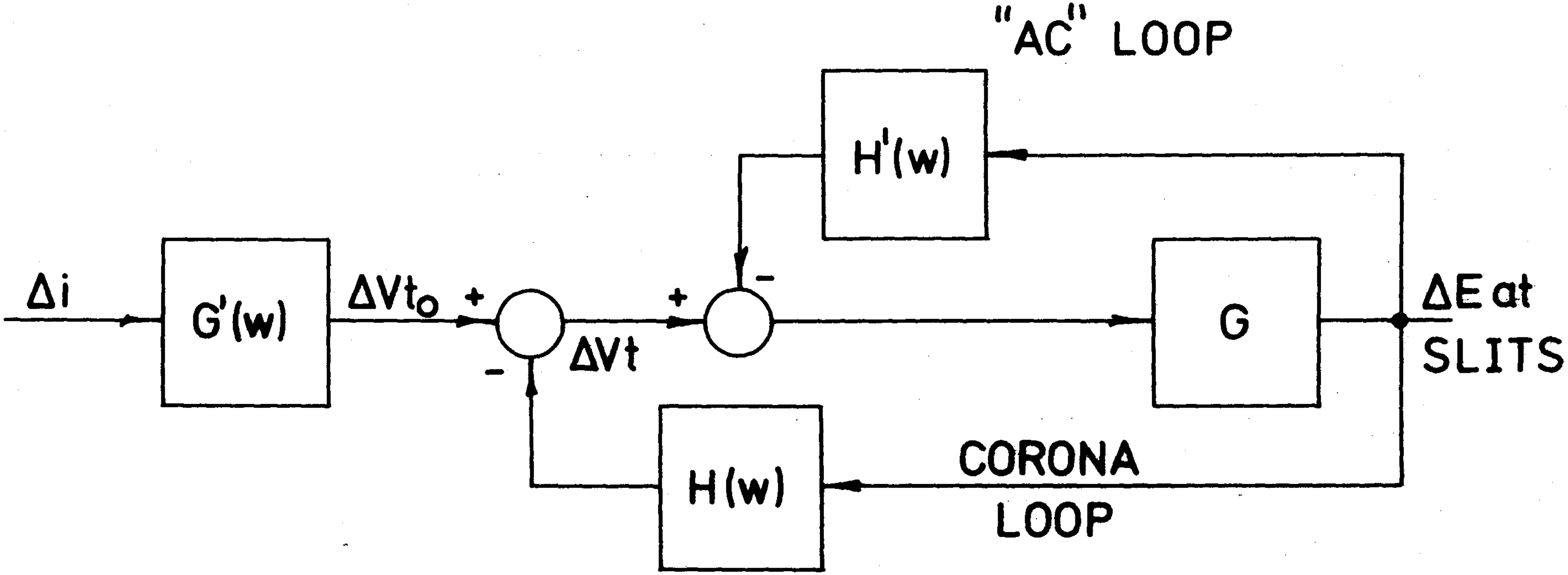

$$Rt = \frac{1}{1 + \dfrac{GH}{1 + GH'}} \qquad Re = \frac{1}{1 + G(H + H')}$$

FIG.2 THE DOUBLE LOOP CONTROL SYSTEM

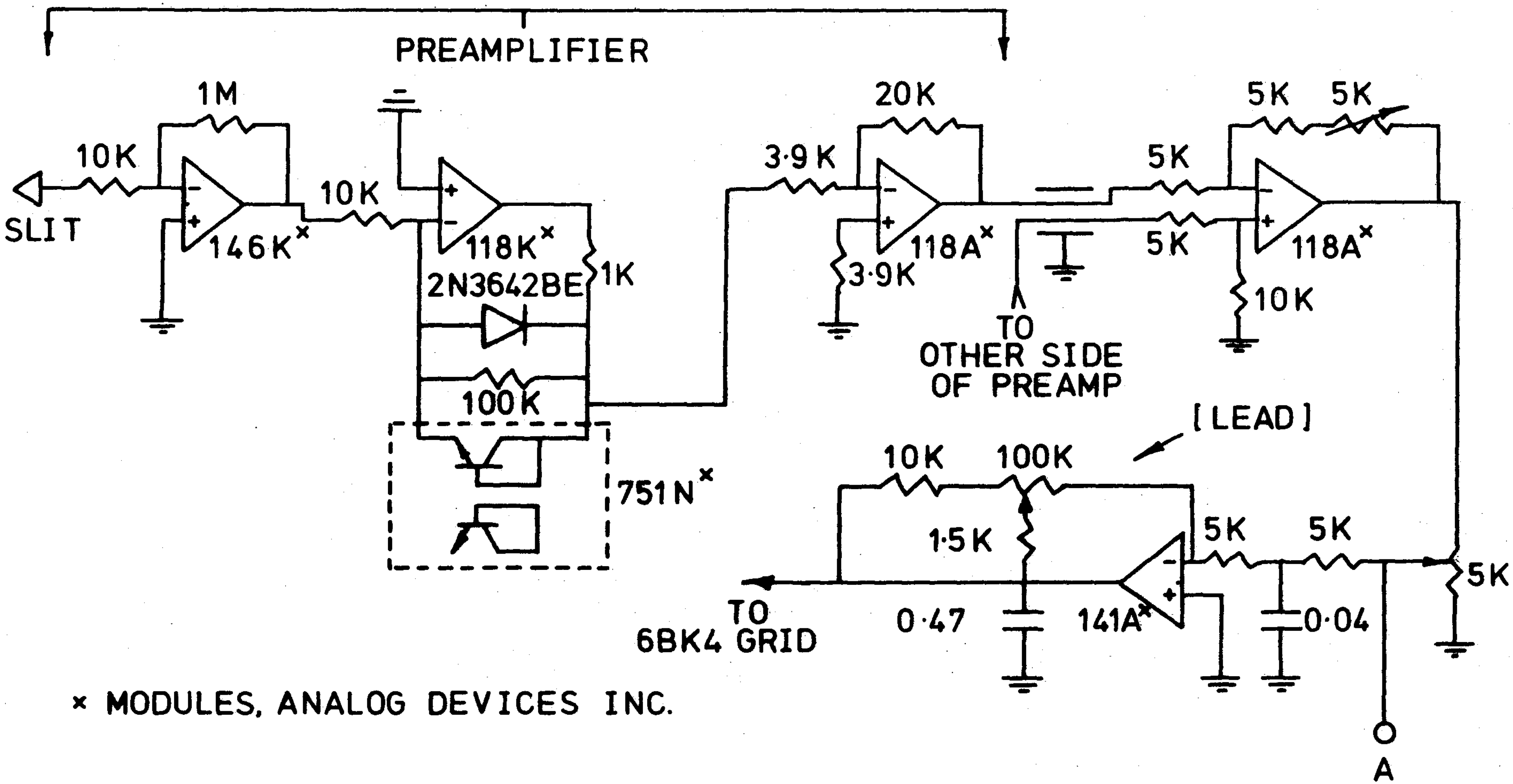

× MODULES, ANALOG DEVICES INC.

FIG. 3 THE CORONA CONTROL LOOP

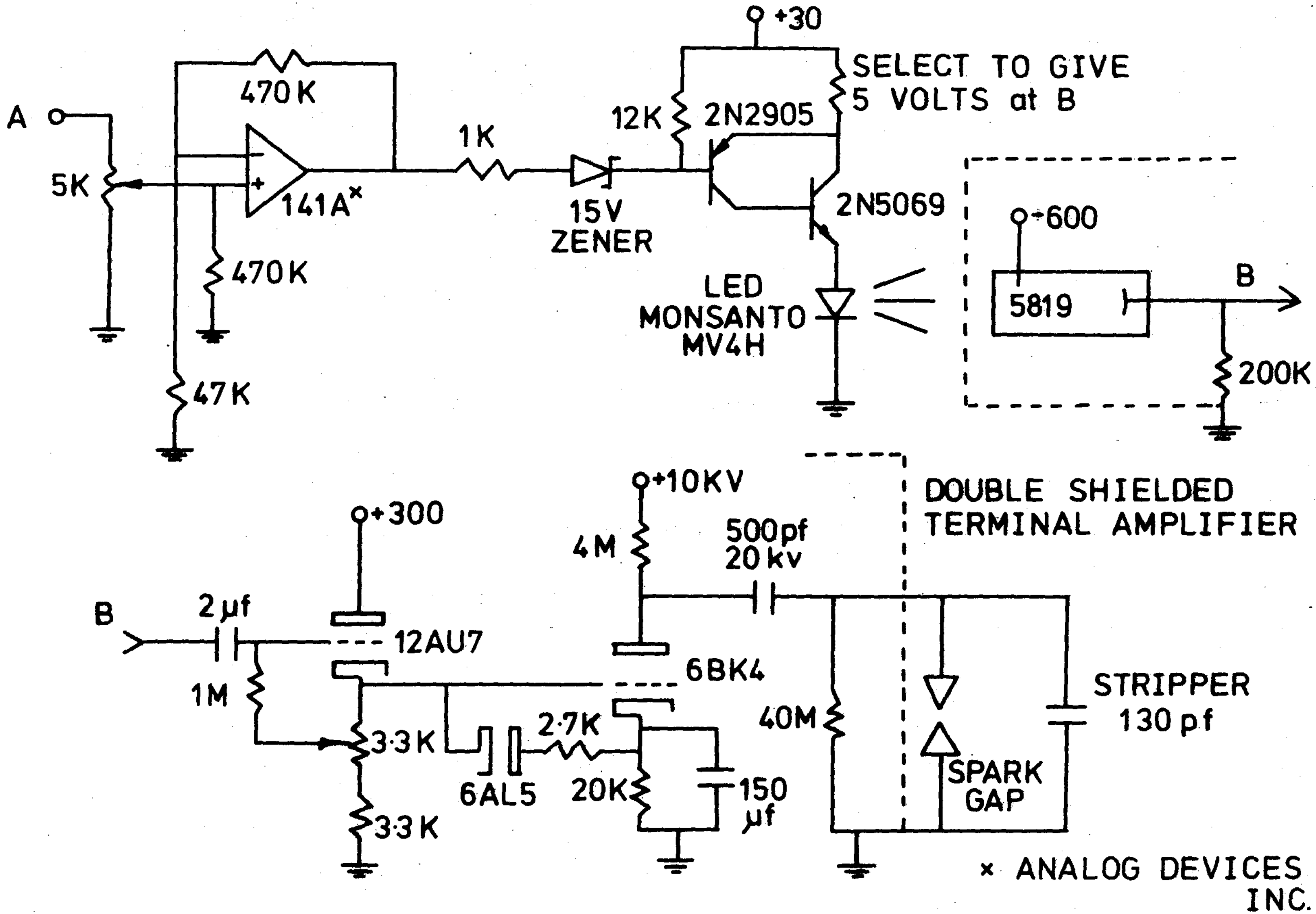

FIG. 4 THE AC CONTROL LOOP

behaviour, and it now becomes useful to display the slit difference signal as well on an oscilloscope.

Since this is a feedback system it is essential to investigate its stability, that is whether the denominators of Rt and Re approach zero at any angular frequency ω. One of the most straightforward ways to do so is to present Bode plots (gain phase versus angular frequency ω) of G(H+H') and GH/(1+GH'). These are shown in figures 5 and 6 respectively, for a lead frequency ($\omega 4$) of 210 Hz. The variable K is defined at ω=10 Hz as:

$$K = \frac{|GH'|}{|GH|} .$$

The Bode plot of the corona loop alone, that is the Bode plot of G(H+H') for K = 0.0, is shown in figure 7 as a function of the lead frequency ω_4. This plot was used to fix the value of ω_4 at 210 Hz in figures 5 and 6, since this value produced the maximum stable gain at the belt frequency ω = 10 Hz. Referring to figure 5 one sees that an additional 52 db of stable gain is available at 10 Hz. Also one notes that large values of K are neither necessary nor desirable. At the optimum value, the AC loop has only sufficient gain to provide the phase margin desired in the critical region near 100 Hz angular frequency.

From figure 6 one finds that for these small values of K, the terminal will behave in a similar manner to the limiting

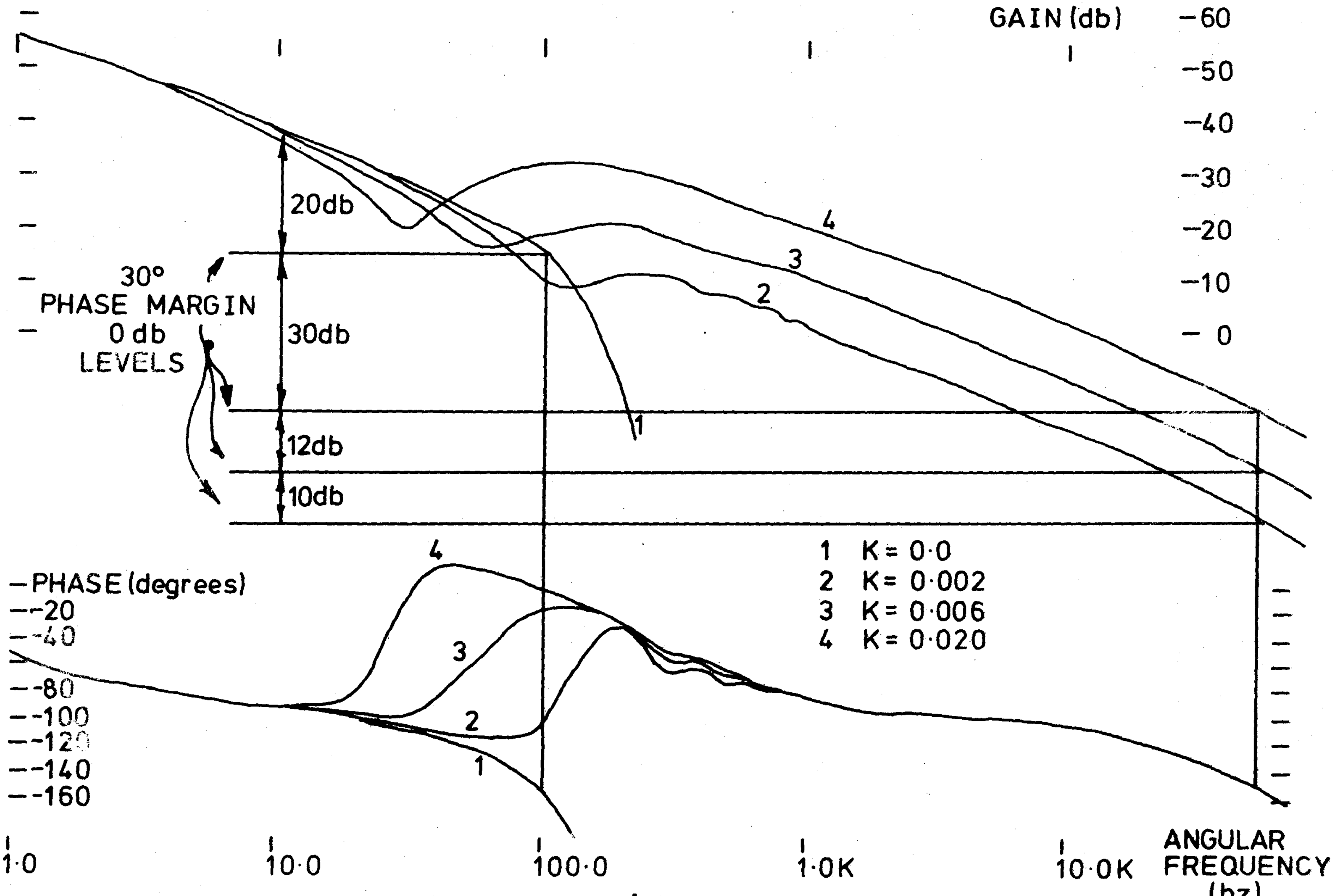

FIG.5 BODE PLOT OF G(H+H')

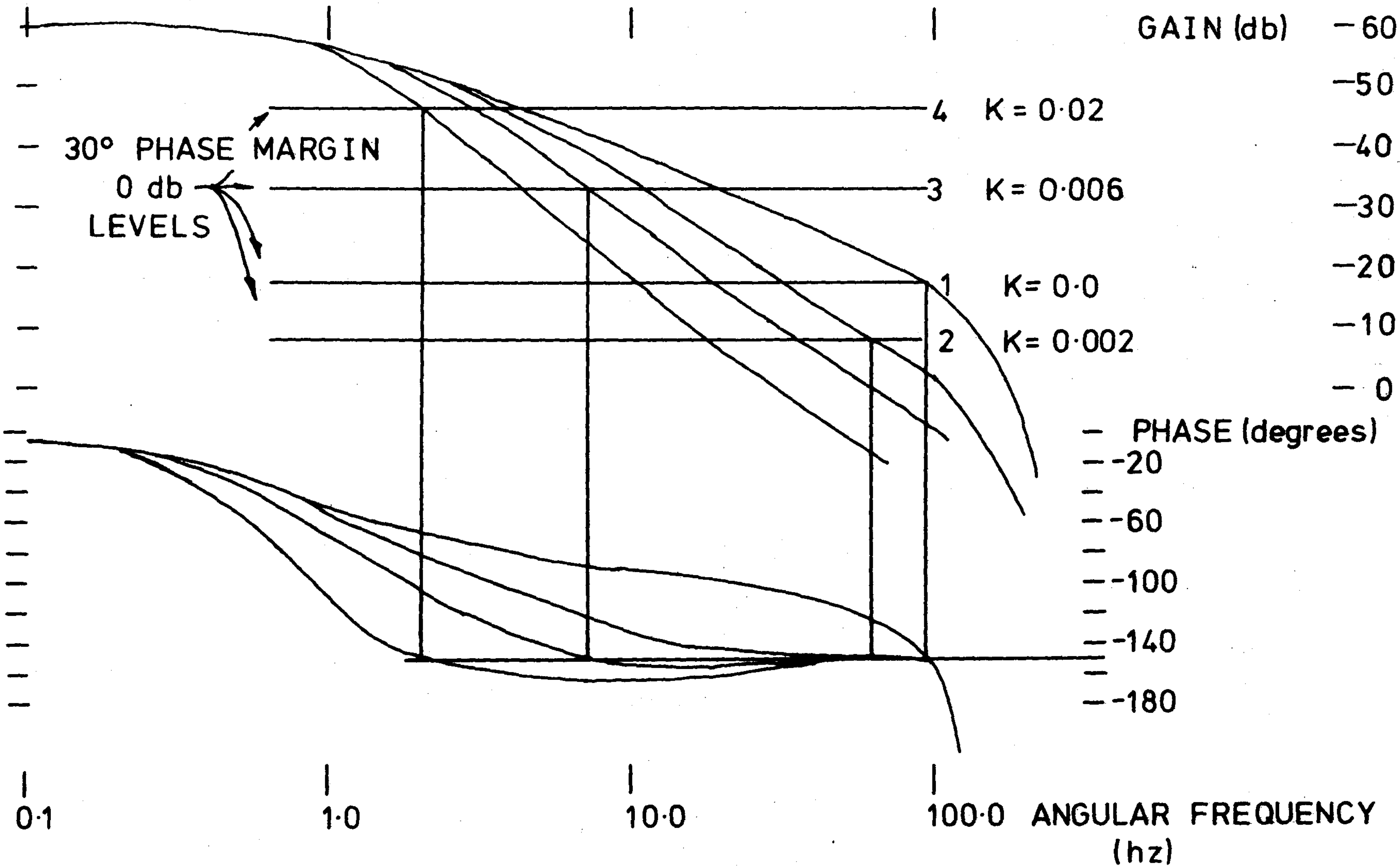

FIG. 6 BODE PLOT OF GH/(1+GH')

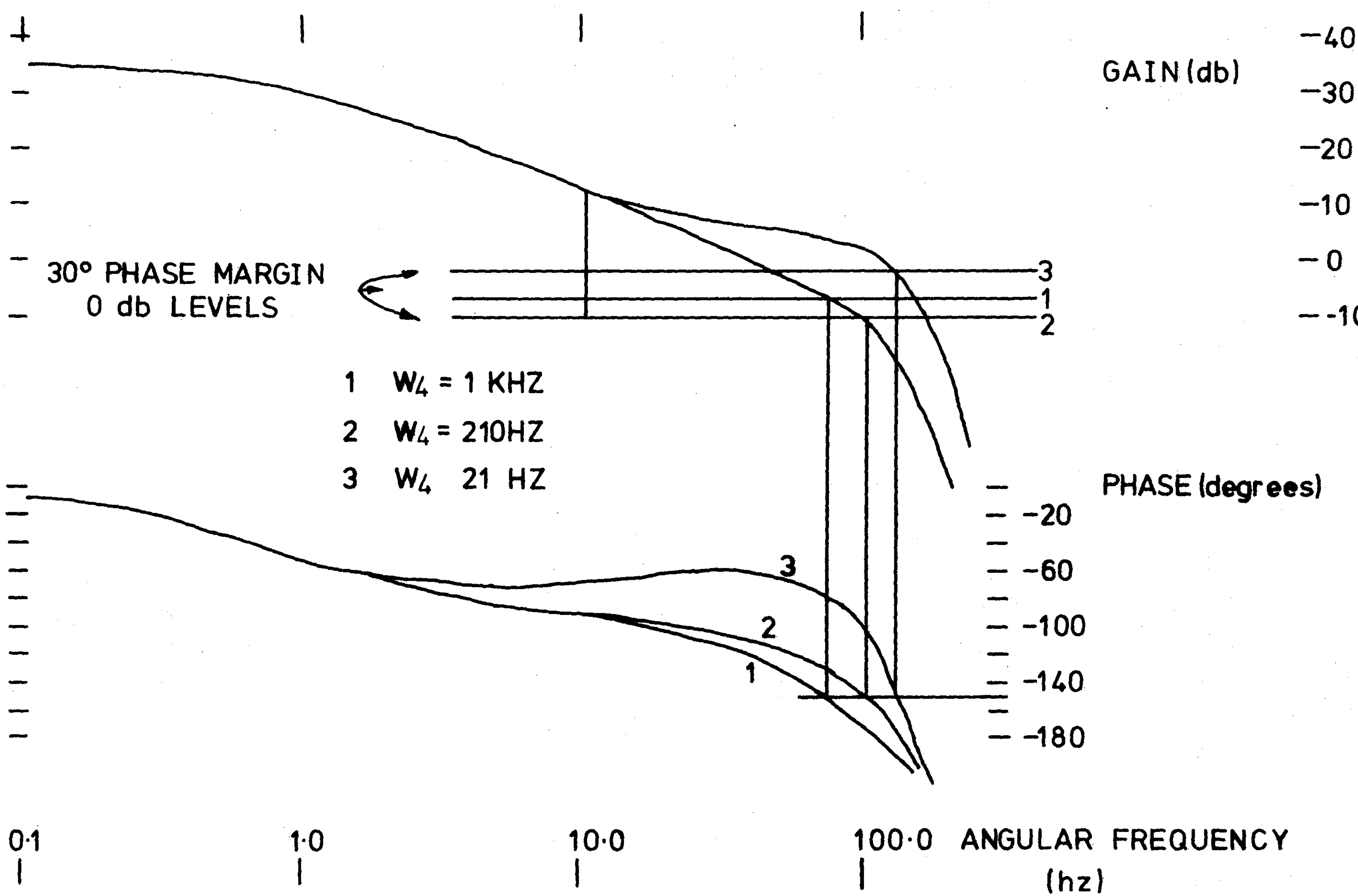

FIG.7 BODE PLOT OF GH

case where K = 0.0. One then expects several kilovolts of terminal ripple as mentioned earlier. This is essential information, as the terminal amplifier must be designed with the capability of nulling these fluctuations.

Although the Bode plots indicate that the inclusion of the 2nd feedback loop should essentially eliminate any terminal voltage ripple, one does not expect such a dramatic effect on the overall resolution. The feedback controls only the coherent energy spread, that is the slow modulations resulting from voltage ripple on the terminal, or on the ion source power supplies. However, incoherent effects such as straggling in adder gas and stripper, and Doppler broadening from thermal motion in the target remain.

Collins et al[7)] measured $\sim$ 200 eV FWHM spread from an ion source similar to the one used on the McMaster tandem. Their measurement included both the thermal energy spread of the negative ions extracted from the duoplasmatron, and straggling in the adder gas. Allison[8)] reports the optimum thickness of hydrogen adder for conversion of 15 keV H^+ ions to H^- ions to be 10^{-2} $\mu g/cm^2$. This corresponds to an energy loss of approximately 40 eV. For such a thin stopper the statistics of the stopping process are very poor and the energy profile of the beam emerging from the stopper is very skewed. One then expects the straggling FWHM to be approximately twice the energy loss or 80 eV.

In a further paper[9] Collins reports a width directly from a duoplasmatron of 8-50 eV FWHM, depending on the arc current and the magnetic field. One would then conclude that the total source width will be in the range of 100 to 200 eV depending mainly on the adder thickness.

Generally one employs a thin, self-supporting carbon foil for stripping hydrogen or helium. For a 10 $\mu g/cm^2$ carbon foil, this will cause $\sim$ 260 eV FWHM[10] straggling. Alternatively one can use a thin gas stripper, and have control over its thickness. A rough estimate of the thickness necessary can be made as follows. Allison gives the crossection for charge exchange of 200-400 keV hydrogen in oxygen as

$$\sigma(\text{negative to neutral}) = 34.4\times10^{-17}\ cm^2/\text{atom}$$

$$\sigma(\text{neutral to positive}) = 19.0\times10^{-17}\ cm^2/\text{atom}.$$

The crossections will fall off approximately as the stopping power with increasing energy as the same processes contribute to the stopping. Then at 7 MeV the stripping crossection will be $\sim 10^{-17}\ cm^2$/atom. A 5 $\mu g/cm^2$ thick oxygen stripper will then strip $\sim$ 80% of the beam. The energy loss and straggling in the gas will be 250 eV and 130 eV FWHM respectively.

These figures for straggling in the source adder and the stripper are representative of ideal running conditions for the maximum production of beam. If one desires, the resolution broadening from these sources could be decreased at the expense of beam current.

The thermal motion in the target results in an equivalent energy distribution with

$$E_D(\text{FWHM}) = 3.3[MmEkT_{eq}/(m+M)^2]^{1/2} \quad ^{6)}$$

where m is the mass of the incident particle, M is the mass of the target particle, k is Boltzmann's constant, E is the beam energy and T_{eq} is the equivalent target temperature corresponding to the mean energy per vibrational degree of freedom for a solid target. For 14 MeV protons on ^{12}C ΔE_D(FWHM) is 700-1000 eV[6] depending on what assumptions one makes for T_{eq}. This is seen to be a major contribution to the resolution for high energy beams.

However the Doppler width is not an insurmountable problem as demonstrated by Parks et al[11] using a cryogenic target, and Müller et al[12] using an atomic beam target. Collins[7] measures the FWHM of the energy of negative ions extracted directly from a duoplasmatron to be in tens of eV range, depending on gas pressure and arc current in the source. The possibility then exists of reducing the incoherent contributions to the resolution width to the point where the coherent effects would dominate without the AC control loop proposed here.

CHAPTER II

DESIGN DETAILS

Most of the circuitry of the control system employs standard operational blocks. However some considerations deserve special attention.

The preamplifier shown in figure 3 is built in three cascaded stages to obtain a high gain bandwidth product. Placing the log conversion stage after a current gain of one hundred stage lowers the dynamic impedance of the log feedback diodes, since this impedance varies directly as the current in the diodes. The 100 kilohms resistor puts an upper limit on the closed loop pole time constant associated with the diode impedance. The final voltage gain stage provides a high signal level in the cable from the analyzing magnet area to the control room. This cable is a shielded twisted pair to reduce the air loop pickup. Loop pickup is objectionable since it produces a noise signal of opposite polarity at each input to the difference amplifier.

There are several reasons for using a log response preamplifier. It reduces the sensitivity to intensity modulations of the beam since the difference amplifier output is proportional to $\log I_A - \log I_B = \log(\frac{I_A}{I_B})$. Also the log response linearizes the signal on large beam deviations, and avoids the necessity of range changing for different current levels.

The phase lead network, as shown in the Bode plot of GH, partially compensates for the effects of terminal capacity and corona transit time. Since the optimum setting depends on machine voltage and corona point position, this is left as a free variable. The optimum setting is readily found by observing the terminal ripple using the capacitive pickup monitor. High frequency overload of the corona tube caused by too much lead can easily be detected by watching for an increase in the DC corona current as shown by the usual panel meter.

The terminal amplifier shown supercedes a prototype model that employed a miniature high voltage tube at the output. The actual system tests to be described in the next section were made on this prototype. It performed adequately except for a sensitivity to overvoltages during terminal sparking which led to failures after a few months of operation. No special effort was made to shield this prototype amplifier. From experience gained with the prototype we conclude that no small wattage resistors should be used in the output section, and that the output tube should be as large as physically possible. A 6BK4 would seem a good choice. The high voltage capability of this tube should allow the protective spark gap to fire before the tube breaks over. Also the 6BK4 is capable if dissipating considerable energy itself. Since it is necessary to employ a low plate voltage to keep to a minimum the physical size of the amplifier and power supply, the 6BK4 has to be run at positive grid bias. Thus a 6AL5 is included to reduce bias drifts due to signal rectification. The output is AC coupled to reduce the maximum positive voltage applied to the stripper gas canal, thus avoiding discharge in the gas. Since a 6 db per octave "rolloff" was desired, this was provided by the output coupling.

One additional mechanical change was found of great value. Examination of the slit signals showed that secondary electrons were collected by alternately one slit, then the other as the beam shifted between the analyzing slits. This effect displayed a threshold behaviour producing a nearly square wave output at the difference amplifier. Due to the close proximity of the two slits in the suppression cage, it was found that even as much as three kilovolts of suppression voltage was not sufficient to eliminate this behaviour. Collection of the secondary electrons by the cage proved more useful, but this was rejected as a solution since the output would still depend strongly on the secondary emission characteristics of the slits. The final solution adopted was to separate the two slits along the beam axis in individual suppression cages[†]. This was easily done using an additional set of "shadow" slits supplied with the accelerator.

[†]Thanks to Phil Ashbaugh for first suggesting this solution.

CHAPTER III

SYSTEM TEST

The improvement in system performance is demonstrated in two ways. In the first of these the slit difference signal is monitored with and without the terminal amplifier in operation. In Figure 8A are shown oscilloscope traces of the terminal voltage at the top, and the slit difference signal at the bottom. The upper trace corresponds to 2 kilovolts per division. In figure 8b is shown the effect of turning on the terminal amplifier, which also allows the corona loop gain to be increased. It is evident that a considerable improvement has been obtained. The 16 db reduction in slit error signal corresponds to the additional 16 db of corona loop gain. The terminal voltage ripple of approximately 1 kilovolt FWHM should then be reduced to an effective value of 160 volts FWHM. These photographs were obtained at a time when 13 MeV alphas were being accelerated.

The second test of the system was carried out under actual operating conditions. At a beam energy of 14.2 MeV the influence of the beam resolution was observed on the yield curve of protons scattered elastically at 135 degrees lab angle from a thin (10 $\mu g/cm^2$) carbon foil. This energy corresponds to the first T = 3/2 level of ^{13}N. This level has a natural width of 1.22 keV known from other sources[4,5]. The high machine voltage

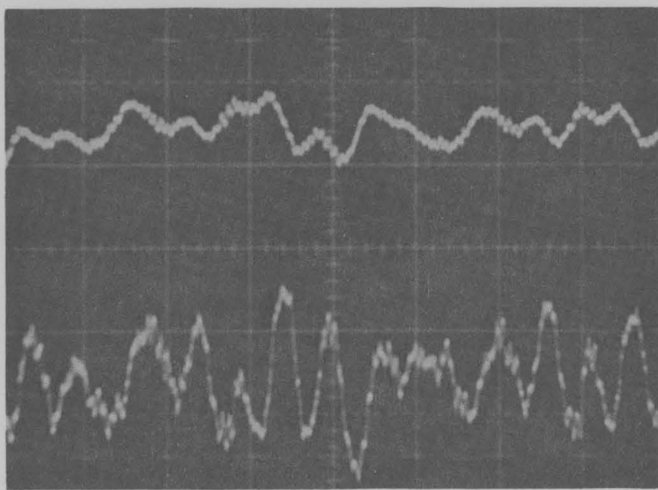

100 ms, division

a) TERMINAL AMPLIFIER OFF

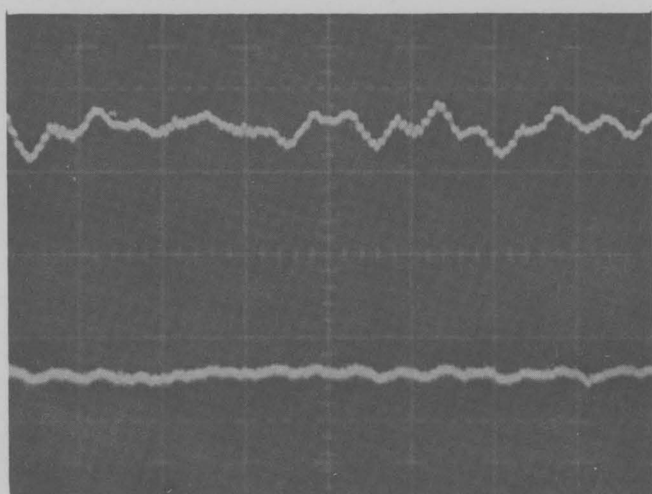

100 ms, division

b) TERMINAL AMPLIFIER ON

FIG. 8 SCOPE MONITOR OF THE TERMINAL VOLTAGE (upper trace, 2kv/division); AND THE SLIT DIFFERENCE SIGNAL (lower trace, 10 v/division) of 7.1 MV required provides a severe test of the control system, since the open loop voltage fluctuations tend to increase with the machine voltage.

The resulting yield curves over the region of the resonance are shown in figure 9. The negative ion source (NIS) and high energy (HE) pressures are related to the adder and stripper thicknesses respectively.

As discussed in Chapter II the straggling in the adder is less than 200 eV FWHM and the straggling in the stripper is less than 130 eV FWHM. Since these widths are added in quadrature to the other contributions to the total resolution, the difference between runs 1 and 3 should be at most 0.01 keV. The observed difference is then a measure of the repeatability of the fits. Then comparing runs 1 and 3 with run 2 there is seen to be a significant difference. The terminal amplifier has removed a coherent width of $(2.4^2 - 1.8^2)^{1/2} = 1.6$ keV FWHM. Folding together the separate widths of a) the source, 200 eV FWHM, b) the stripper, 130 eV FWHM, c) the target doppler width 700-1000 eV FWHM, d) the natural width of 1220 ev FWHM, e) the coherent width of 1600 eV FWHM and f) the target thickness 300 eV, one obtains a total width of 2160 to 2270 eV FWHM, not inconsistent with the observed width in run 2.

One can definitely say that stripper modulation is a promising technique to improve the resolution of tandem accelerators.

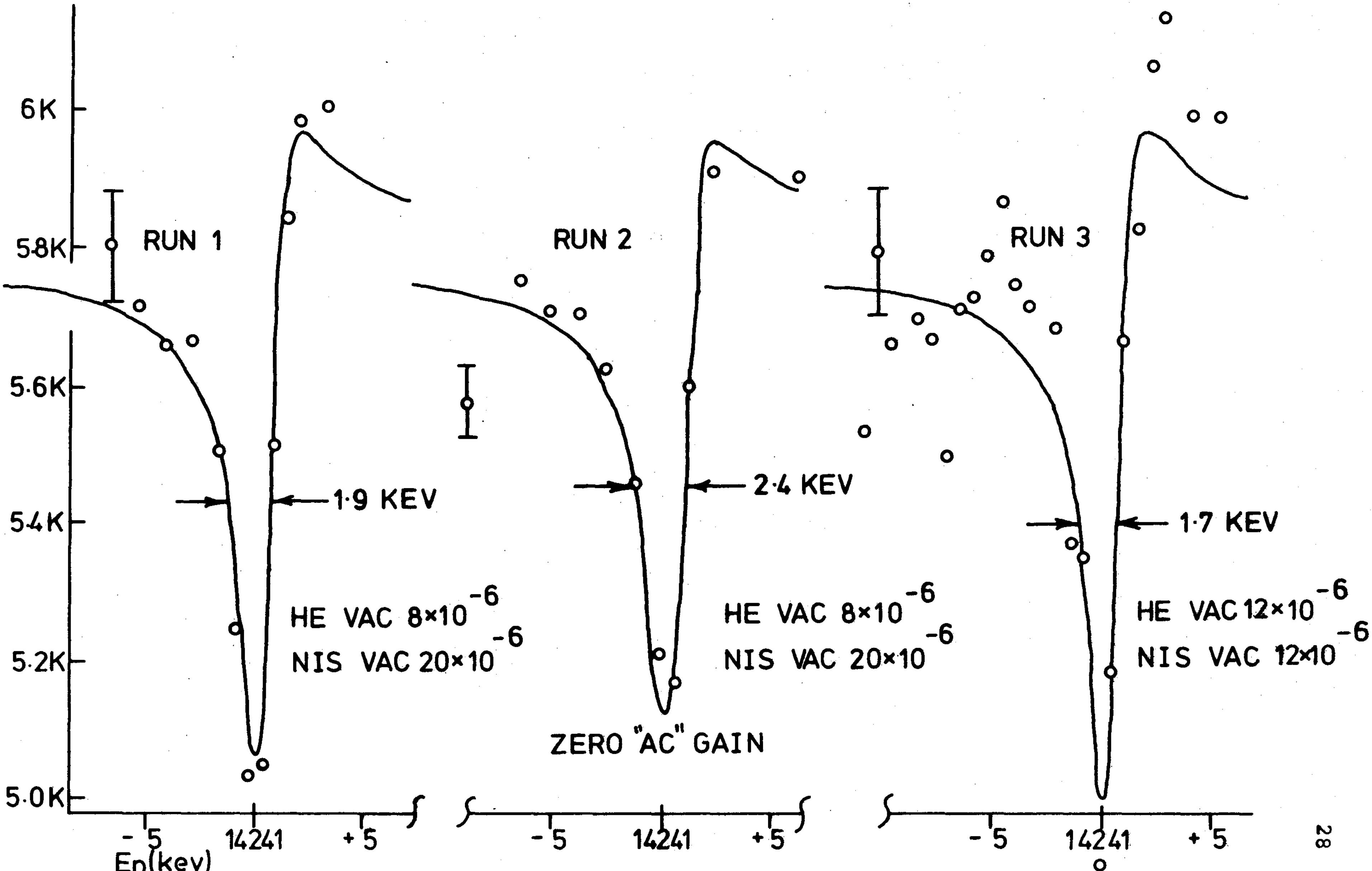

FIG. 9 YIELD CURVES AT "14·231" MEV RESONANCE, $\theta_L = 135°$

APPENDIX A

The propogation of an error from Y(E) and F(E) to σ(E) can be calculated directly. Partitioning the expression for Y(E) one can write:

$$Y(i) = \sum_j \sigma(j) F(i,j)$$

$$dY(i) = \sum_j d\sigma(j) F(i,j) + \sum_j \sigma(j) dF(i,j).$$

In matrix notation:

$$\underset{\sim\sim}{dY} = \underset{\sim}{F}\, d\underset{\sim}{\sigma} + \underset{\sim\sim}{dF}\, \underset{\sim}{\sigma}$$

$$d\sigma = \underset{\sim\sim\sim}{F^{-1}}\, \underset{\sim\sim}{dY} - \underset{\sim\sim\sim}{F^{-1}}\, \underset{\sim\sim}{dF}\, \underset{\sim}{\sigma} .$$

Replacing differentials by error and reverting to the summation in order to determine the coefficients of each error term:

$$\Delta\sigma_i = \sum_{j=1}^{M} F^{-1}_{ij} \Delta Y_j - \sum_{k=1}^{M} \sum_{j=1}^{M} (F^{-1}_{ik}\sigma_j) \Delta F_{ij} .$$

If one repeats the measurement N times and sums the squares of the errors $\Delta\sigma_i$, one has the variance of σ_i. In this sum cross terms such as $\Delta Y_i\ \Delta F_{k_j}$ will vanish if N is large as there is no correlation between ΔF_{k_j} and ΔY_i. However one must remember that $F_{k_j} = F_{k+L,j+L}$. One then has for the variance of σ_i

$$S^2[\sigma_i] = \sum_{j=1}^{M} (F^{-1}_{ij})^2 S^2[Y_j] + \sum_{k=1}^{M} \sum_{j=1}^{M} \Big(\sum_{L=0}^{M-\mathrm{Max}(k,j)} (F^{-1}_{i+L,k+L}\sigma_j)^2 \Big) \times S^2[F_{k_j}]$$

where

$$F_{k_j} = \sum_{p=1}^{N} G_{k,p} \frac{\Delta}{N}$$

$$S^2[F_{k_j}] = \left(\sum_{p=1}^{N} \frac{G_{k,p}}{N}\right)^2 S^2[\Delta] + \frac{\Delta}{N} \sum_{p=1}^{N} S^2 G_{k,p} \ .$$

One could proceed from these expressions to calculate $S^2[\sigma_i]$. However the complexity of this calculation which grows as M^3, and the fact that $\underset{\sim}{F}$ becomes more ill conditioned as the width G(E) increases, (or the partition interval decreases) would seldom justify the effort.

APPENDIX B

The Laplace transform of f(t) is defined:

$$L[f(t)] = \int_0^{\infty} f(t)e^{-st}dt = F(s)$$

if $f(t) = 0 \quad t < 0$,

where s is in general a complex variable. The Laplace transform has the following very useful properties:

1) $L[\frac{df(t)}{dt}] = sL[f(t)] - f(0^+)$

$$= sF(s) - f(0^+)$$

2) $L[\int_0^t f(t)dt] = \frac{L[f(t)]}{s}$

$$= \frac{F(s)}{s}$$

3) $L[f(t-\tau)] = e^{-s\tau}L[f(t)]$

$$= e^{-s\tau}F(s)$$

4) $L[\int_0^t u(x)g(t-x)dx] = L[u(t)]*L[g(t)]$

$$= U(s)*G(s)$$

5) $L[f_1(t) + f_2(t)] = L[f_1(t)] + L[f_2(t)]$

$$= F_1(s)+F_2(s)$$

If in property 4) for any linear system u(t) is the input, g(t) is the response at time t to a unit impulse at t=0, then by superposition $\int_0^t u(x)g(t-x)dx$ is the output at time t. Then one can write simply $V_{out}(s) = U(s)G(s)$.

Similarly for a staged system of n blocks, one can write:

$$V_{out}(s) = U(s) * \prod_{i=1}^{n} G_i(s).$$

It is then convenient to introduce the transfer function

$$G(s) = \frac{V_{out}(s)}{U_{in}(s)} .$$

Since for a capacity C, and an inductance L

$$v_c(t) = \frac{1}{c}\int i_c dt \ , \ V(s) = \frac{I(s)}{sc}$$

$$v_L(t) = L\frac{dv_L}{dt} \qquad V(s) = LsC$$

one can define a complex impedance which is:

$$Z_x(s) = \frac{L[V_x(s)]}{L[I_x(s)]} .$$

Then by property 5) in any series string of circuit elements where:

$$v_{out}(t) = \sum_{\ell=1}^{n} v_{element_\ell}(t)$$

$$V_{out}(s) = \sum_{\ell=1}^{n} V_{element_\ell}(s)$$

$$V_{out}(s) = \sum_{\ell=1}^{n} I_{element_\ell}(s) Z_{element_\ell}(s)$$

$$= I(s) \sum_{\ell=1}^{n} Z_{element_\ell}(s) \quad .$$

This expression is analogous to $V_{out} = i \sum_{\ell=1}^{n} R_\ell$ for a purely resistive network. Without further explanation it is probably clear that for any network

$$Z_{total}(s) = \frac{V(s)}{I(s)}$$

can be found by the well known rules used for combining impedance in series or parallel.

The usefulness of the transfer function is now more apparent. Since it is easily obtained as $Z_{total}(s)$, the system response is also readily obtained as

$$v(t) = L^{-1}[I(s)Z_{total}(s)].$$

This inverse transformation is facilitated by applying tables of transform pairs. Furthermore if the input is sinusoidal current of unit amplitude and frequency ω, one has in the limit of large t

$$\underset{t\to\infty}{v(t)} \to |G(j\omega)|\sin[\omega t + \angle G(j\omega)]$$

where $j = \sqrt{-1}$. Hence G(s) also yields the frequency response of the system, that is, the gain and phase of the output as a function of the frequency of a sinusoidal input. This quantity can be used to determine the stability of a feedback system, since the output must never be fed back (transferred) to the input with more than unity gain if it is in phase with the input. If this condition is not met as determined from the frequency response, generally shown as a Bode plot of gain in decibels and phase in degrees versus frequency, then the system will oscillate.

Properties 2) and 3) can be combined for the specific case required:

$$f(t) = \int_{0}^{t-\tau} g(x)\,dx$$

$$L[f(t)] = \int_{0}^{\infty} \int_{0}^{t-\tau} g(x)\,dx\; e^{-st} dt \; .$$

Integrating by parts:

$$L[f(t)] = \int_{t=0}^{t=\infty} \frac{e^{-st}}{-s} \int_{0}^{t-\tau} g(x)\,dx + \int_{0}^{\infty} \frac{e^{-st}}{s}\, g(t-\tau)\,dt$$

$$= \frac{1}{s} \int_{0}^{-\tau} g(x)\,dx - \frac{1}{s} \int_{0}^{\infty} g(x)\,e^{-sx}\, \frac{e^{-\infty}}{e^{-sx}}\, dx$$

$$+ \frac{1}{s}\, L\, [g(t-\tau)] \; .$$

The first term on the RHS is 0 as $g(x) = 0$ for $x < 0$. Since $\int_{0}^{\infty} g(t)e^{-st}\,dt = L[g(+)]$ is finite, the 2nd term is seen to vanish

$$\therefore \quad L[\int_{0}^{t-\tau} g(x)\,dx] = \frac{1}{s}\, L[g(t-\tau]$$

$$= \frac{e^{-st}}{s}\, L[g(t)] .$$

It is now possible to derive the transform function from the grid of the corona tube to the terminal.

For any body of charge Q and voltage v one can write:

$$Q = cv$$

where c, the capacity is a geometry dependent term. Then by partial differentiation

1(b) $$\frac{\partial v}{\partial t} = \frac{1}{c}\frac{\partial Q}{\partial t}\bigg|_{c} - \frac{Q}{c^2}\frac{\partial c}{\partial t}\bigg|_{Q}$$

Only the first term on the right hand side is applicable in discrete element systems. However, here where one must consider the ion drift in the SF_6 gas and consequent change in charge geometry resulting from this "displacement current", the second term is also required. If Q represents a drifting charge,at potential v, in the SF_6 gas, τ is the ion transit time from the corona points to the terminal, then one has from energy considerations, in the case of constant terminal charge Q_T:

$$Q_T\, dV_T - QdV = 0$$

$$\left(\frac{dv}{dt}\right)_{Q_T} = -\frac{Q}{Q_T}\frac{dv}{dt}$$

$$\left(\frac{dv}{dt}\right)_{Q_T} = -\frac{Q}{Q_T}\frac{V_T}{\tau}$$

1(c) $$\left(\frac{dv}{dt}\right)_{Q_T} = -\frac{Q}{C_T\tau}$$

where the drift velocity, and hence the field gradient in the SF_6 gas is approximated as a constant. Then 1(c) is the second term in 1(b) above. Note that after a time τ 1(c) demands that $dV_T = -\frac{Q}{C_T}$ as required in the case of a discrete capacitor where the charge enters the element instantaneously. The actual corona circuit is shown in figure 10(a). An equivalent circuit is shown in figure 10(b) which simplifies to the form shown in 10(c). Then recognizing that i is the displacement

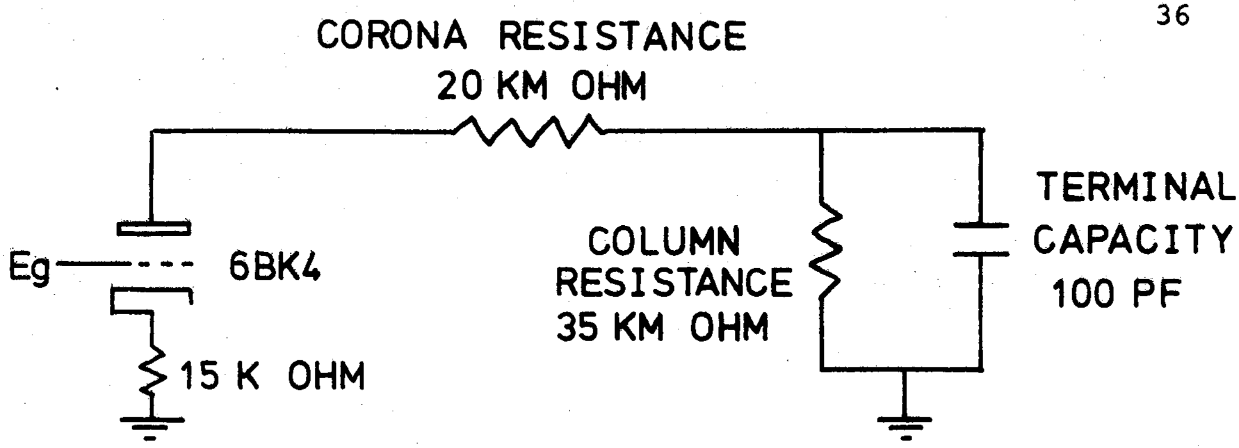

FIG.10(a) THE CORONA CIRCUIT

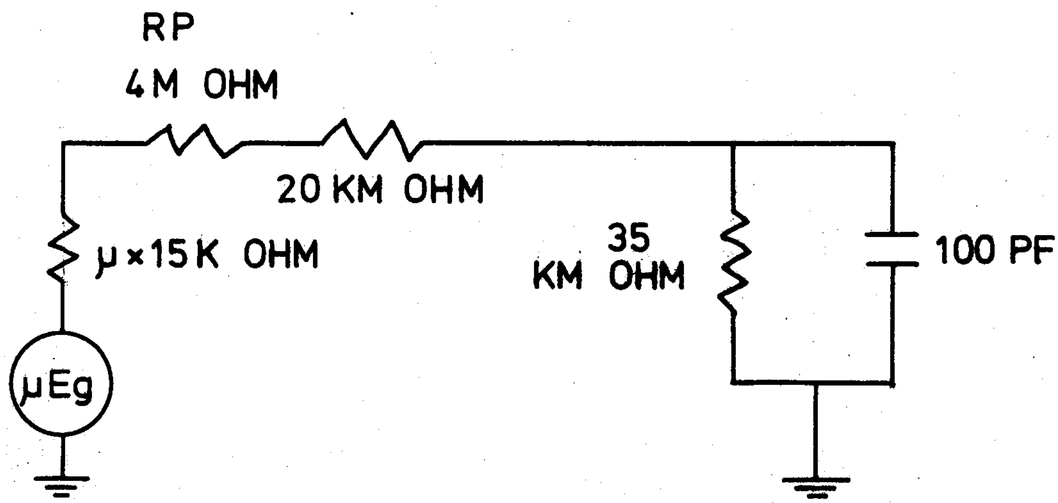

FIG.10(b) EQUIVALENT CIRCUIT

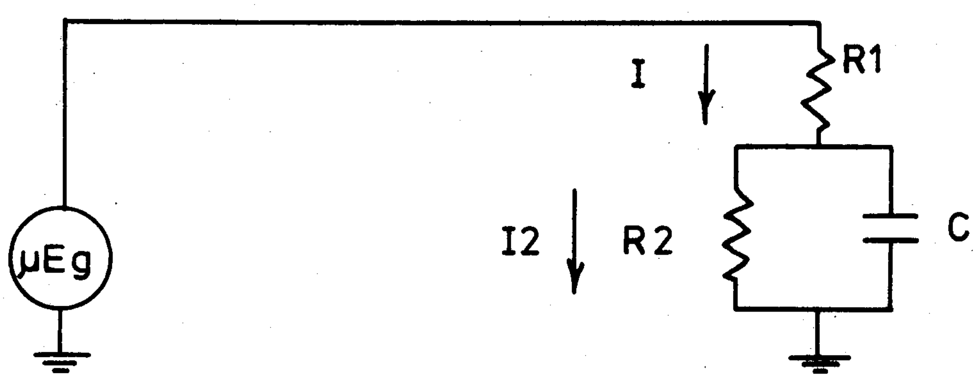

FIG.10(c) SIMPLIFIED CIRCUIT

current whereas i_2 flows into a discrete element:

$$\frac{dv_T}{dt} = \frac{1}{c\tau}\int_{t-\tau}^{t} i\,dt - \frac{1}{c}\, i_2$$

where it is understood that all voltages and currents refer to deviations from equilibrium values. But:

$$I(s) = \frac{\mu eg(s)}{Z_{total}(s)}, \quad Z_{total}(s) = R_1 + \frac{R_2}{1+R_2CS}$$

$$Z_{total}(s) = R_T\left(\frac{1+R_pCS}{1+R_2CS}\right)$$

where:

$$R_p = \frac{R_1R_2}{R_1+R_2} \qquad R_T = R_1+R_2.$$

Then;

$$\frac{dv_T}{dt} = \frac{\mu eg}{c\tau}\int_{t-\tau}^{t} L^{-1}\left[\frac{1}{R_T}\left(\frac{1+R_2CS}{1+R_pCS}\right)\right]dt$$

$$- \frac{v_T}{CR_2}$$

where L^{-1} [F(s)] is the inverse Laplace transform of F(s). Taking the Laplace transform of both sides (see Appendix B)

$$S\, V_T(s) = -\frac{V_T(s)}{CR_2} + \frac{\mu Eg(s)}{R_TC\tau}\left[\frac{1}{S}\left(\frac{1+R_2CS}{1+R_pCS}\right)\right](1-e^{-s\tau})$$

$$V_T(S) = \mu Eg(s)\left(\frac{R_2}{R_t}\right)\left(\frac{1-e^{-s\tau}}{s\tau}\right)\left(\frac{1}{1+R_pCS}\right).$$

Assuming that the slit differential signal is linearly related to beam displacement it is now possible to write the transfer function of the total feedback loop from slit to terminal.

APPENDIX C

The transfer functions employed in generating the Bode plots are given here in detail and the reader may assess for himself whether they adequately describe the system.

$$H = A\ (i+j\omega|\omega_4)\omega_7(1-\cos\ \omega|\omega_7 - j\ \sin\ \omega|\omega_7)/$$
$$[(1+j\omega|\omega_5)(1+j\omega|\omega_6)j\omega(1+j\omega|\omega_8)]$$

$$H' = 2.7A(j\omega)^2/[1+j\omega|\omega_1)^2(1+j\omega|\omega_9)(1+j\omega|\omega_{10})$$
$$(1+j\omega|\omega_{11})]$$

$$A = 1/[(1+j\omega|\omega_1)^3(1+j\omega|\omega_2)]$$

where:

ω_1 = frequency at which closed loop gain of current multiplier meets open loop gain

ω_2 = lowest frequency at which closed loop gain of log converter meets open loop gain

ω_4 = lead frequency variable 21 to 1.6×10^3 Hz)

ω_5 = upper lead frequency

ω_6 = high frequency filter cutoff frequency

ω_7 = corona delay frequency

ω_8 = terminal time constant cutoff frequency

ω_9 = photo multiplier to cathode follower coupling frequency

ω_{10}= output coupling frequency

ω_{11}= output upper cutoff frequency due to load capacity.

References

1) E. A. Gere et al, IEEE Transactions on Nuclear Science, Vol. NS-14, No. 3, 161 (June 1967).

2) W. K. Brookshier et al, IEEE Transactions on Nuclear Science Vol. NS-18, No. 2, 101 (April 1971).

3) R. Bloch et al, Nucl. Instr. and Meth. 59,325 (1968).

4) D.J. Bredin et al in Isobaric Spin in Nuclear Physics, edited by J. D. Fox and D. Robson (Academic Press Inc., New York, 472 (1966).

5) M. J. Levine and P. D. Parker, Phys. Rev. 186, 1021 (1969).

6) T. G. Dzubay et al, Nucl.Instr. and Meth. 101, 407 (1972).

7) L. E. Collins et al, Nucl. Instr. and Meth. 42, 206 (1966).

8) S. K. Allison, Rev. of Modern Phys. Vol. 30, No. 4, 1137 (October 1958).

9) L. E. Collins et al, IEEE Transactions on Nuclear Science, Vol. NS-12, No. 3, 247 (June 1965).

10) N. M. Clarke, Nucl. Instr. and Meth. 96, 497 (1971).

11) P. B. Parks et al, Rev. Sci. Instr., 35, 549 (1964).

12) V. Meyer et al, Physica Acta 37, 611 (1964).